ANALYSIS OF ELECTRIC PROPULSION CAPABILITIES IN ESTABLISHMENT AND KEEPING OF FORMATION FLYING NANOSATELLITES

Eviatar Edlerman[*] *and Igal Kronhaus*[†]

Technion – Israel Institute of Technology, Haifa 32000, Israel

ABSTRACT

Nanosatellite clusters are one of the current and future trends in space technology. In order to maintain a satellite cluster, over a long period of time, the nanosatellites need to mitigate the alongtrack drift created by the initial orbit injection. In the mass range of 1-10 kg, CubeSats have strict constraints on allowed mass, volume, electrical power, and are equipped with only limited sensor and actuator capability. State of the art miniaturized electric propulsion (EP) systems are one option to realize the required orbit control capability. Due to the low thrust provided by an EP system, long orbit control maneuvers are required. Therefore, mission design is highly effected by long-term attitude and power constraints. Assuming a cyclic thrust controller, four methods were developed to allocate the satellite power and attitude resources for orbit control. Two time division methods are developed that allocate dedicated time slots for each of the satellite main tasks. Alternatively, two cosine methods are presented that utilize an error cone, around the required attitude, as a criterion for selecting when to operate the thruster. As a test case a typical deployment scenario was chosen with three 6U CubeSats. The CubeSats are equipped with a 100 N thruster with 1000 s specific impulse. Using a CubeSat power system model and a high fidelity orbit simulation, it was shown that all the resource allocation methods were successful in realizing a CubeSat formation flying mission. The fuel mass consumed was less than 2 g and the maneuver duration was less than 20 days.

Index Terms— Electric propulsion, Nanosatellites, Formation Flying, Constraints

1. INTRODUCTION

Nanosatellites are fully capable satellites with a mass limit of 10 kg. To increase the functionality of these satellites they can be grouped together in a formation and act as a distributed satellite. A distributed space system [1, 2] is a system that include two or more satellites that act together as one, this can increase the reliability and lower the cost compare to monolithic satellite [3]. In order to maintain a satellite cluster over a long period of time it is required that the inter-satellite distances (ISD) between the cluster agents will be controlled. The cluster agents need to mitigate the along-track drift created by the initial orbit injection, using the very limited resources available onboard.

In recent years few formation flying demonstration where conducted. In 2010 the PRISMA mission demonstrated autonomous formation flying of two micro satellites [4, 5]. PRISMA main spacecraft weight 150 kg, delivered 300 W and used a chemical propulsion system with 11 kg of fuel and six 1 N thrusters. In 2014 CanX-4 and CanX-5 [6] demonstrate a formation flying of two 6 kg nano-satellites. Each satellite was equipped with 4 thrusters, 260 g of fuel and I_{sp} of 45 s. The SAMSON mission [7] will also test autonomous formation flying of three 6U CubeSats using four 20 mN thrusters with I_{sp} of 35 s [8, 9].

As satellites become smaller the challenge of finding a miniaturized propulsion system to provide formation flying capabilities increase. Previous studies (for example [10]) show that electric propulsion (EP) can be used for demanding orbit control maneuvers. Miniaturized EP systems offer an advantage over chemical propulsion thrusters by their smaller volume and mass and offer new possibilities for nanosatellite orbit and attitude control [11, 12]. Miniaturized EP systems are an active research field. Several surveys [13, 14] were published showing a variety of technologies with thrust to power ratios and I_{sp} levels. Most of these systems provide low thrust and therefore require long orbit control maneuvers. However mission design is highly affected by long duration orbit control maneuvers that create long-term attitude and power constraints.

In this work new control algorithms for autonomous nano-satellite formation flying using EP are developed. The provided control algorithms can maintain a long term cluster flight of multiple satellite using orbital element feedback. In contrast to previous work [15, 11] that either ignored the mission constraints or assumed that the satellite orientation is dedicated to the orbit control maneuver, this paper will focus on developing a controller that can work under realistic attitude and mission constraints. The paper is organized as follows: Sec. 2 describes the typical spacecraft constraints

[*]Research Staff Member, Distributed Space Systems Lab, Faculty of Aerospace Engineering ,eviatar@tx.technion.ac.il

[†]Assistant Professor, Faculty of Aerospace Engineering, kronhaus@technion.ac.il

on CubeSat mission; Sec. 3 present a robust controller that utilizes low power EP system to reduce the along track drift; Sec. 4 presents four different implementations of the mentioned controller under mission constraints; and finally Sec. 5 present results from a high fidelity numerical simulation using these methods.

2. SPACECRAFT CONSTRAINTS

A spacecraft is composed of several important subsystems (Fig. 1). Ideally we would like to operate these sub-systems without any restriction and without any coupling between them. This ideal assumption is not valid when designing a real satellite mission. Each subsystem is affected by one or more other subsystems and each subsystem adds more constraints to the mission design. In our model spacecraft, subsystems compete for two major resources : electric power and satellite attitude. While a shortage in electric power can be solved by adding solar panels (SP) or increasing battery energy capacity, the satellite attitude is restricted by the kinematics of a constrained rigid body. We can divide these constraints into short-term and long-term constraints. Short-term constraints have minimal impact on other mission tasks and therefore will be ignored in this paper. In contrast, long-term constraints can be imposed for days or even months and can interfere with other critical tasks.

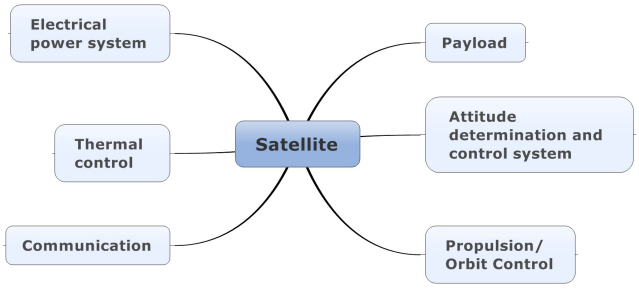

Fig. 1. Schematic view of critical satellite subsystems

As a "hard constraint" we define a constraint that cannot be violated and a "soft constraint" we define as a constraint with some allowed error. In this section we will examine the constraints in different aspects of the mission. Although constraints act on all types of spacecrafts, in this paper we will focus on CubeSats [16, 17].

2.1. Spacecraft structure constraints

The CubeSat structure is a off the shelf component and therefore considered as a hard constraint. Based on the CubeSat design specification [17] the basic unit, known as 1U, has a volume of $1000\,\mathrm{cm}^3$ and a mass limit of 1.33 kg. We can derive from the basic unit the physical limits for the bigger models (Table 1). These physical limitations are taken into account as hard constraints for the mission design. Limited volume and mass will affect subsystem and overall performance of the satellite.

An off the shelf structure also pose a challenges on subsystem placement. One example is the problem of placing SP and nadir pointing payload on a 6U CubeSat. If the β angle (between the orbit plane and the sun vector) is low ($\beta < 10°$) then placing the SP and payload on the opposite side of the same axis is favorable. On the other hand, if $\beta > 80°$ then it is favorable to place the payload normal to the SP. Different placement configurations can affect the performance of the proposed methods. For example a sub-systems placement can be described by using a body-fixed coordinate system $\mathcal{B}$ as shown in Fig. 2. Here we assume that the CubeSat in this paper have the following configuration: deployable solar panels (DSP) are in $\mathbf{z}_{\mathcal{B}}$ direction, thrusters are in the $\mathbf{x}_{\mathcal{B}}$ direction and the payload is pointing towards the $-\mathbf{z}_{\mathcal{B}}$.

Table 1. Physical and power constraints

Model	Mass [Kg]	Volume $[\mathrm{cm}^3]$	SP power [W]	Battery capacity [Wh]
1U	1.33	1000	10	19.24
3U	4	3000	26	38.5
6U	8	6000	40	77

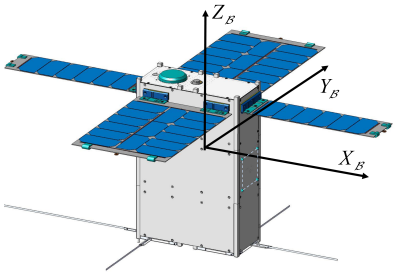

Fig. 2. Structure and body frame directions

2.2. Attitude constraints

A requirement of pointing one of the satellite axis to a specific direction allows only one rotational degree of freedom (DOF). By fixing two of the satellite axes we fully determine the satellite attitude. Therefor at any given moment, the satellite can only achieve one hard constraint and one soft constraint. Another possible option is to fulfill two soft constraints in parallel.

Tracking approximately inertially fixed vectors like the sun vector is similar to tracking a non-moving target. Tracking a non-inertial vector, for example the nadir vector, is more challenging task for an attitude determination and control system (ADCS) and is similar to tracking a moving target. In this case the ADCS has to constantly rotate the satellite axes to keep tracking the target. One example is a case where $\hat{\mathbf{x}}_{\mathcal{B}}$ is pointing to the sun vector $\hat{\mathbf{s}}$ and $\hat{\mathbf{z}}_{\mathcal{B}}$ point towards the ecliptic normal. Because both vectors are approximately inertial the satellite keeps a constant attitude. Considering a case where $\hat{\mathbf{z}}_{\mathcal{B}}$ is pointing to the nadir direction and $\hat{\mathbf{x}}_{\mathcal{B}}$ point towards the orbit normal, in near circular orbit, the expected angular rate is equal to the mean motion $n \triangleq \sqrt{\frac{\mu}{a^3}}$ and the satellite will rotate around $\hat{\mathbf{x}}_{\mathcal{B}}$ at the same rate. A fast angular velocity change can also occur during transition between two different orientations. With limited volume and power, ADCS on CubeSats might not be a able to provide the required angular rate. To avoid using unrealistic control effort, in this paper, we will limit the angular rate to a maximum of $1\frac{\text{deg}}{\text{s}}$.

2.3. Electrical power constraints

Based on the work presented in [18] the two right columns of Table 1 show the maximum solar generated power of 1U, 3U and 6U CubeSats. Here we assume that the solar cells have 28.3 % efficiency and provide 1367 $\frac{\text{W}}{\text{m}^2}$ (@100° C) at their beginning of life. Each 1U panel can carry up to two cells therefore a 3U panel can carry up to 6 cells and a 6U panel can carry up to 12 cells. Some of the more advanced DSP [19] can generate even more power. Here we assume that the DSPs are all on the same plane, pointed to the same direction with a configuration of 4 deployable and 1 body mounted SP. During eclipse the satellite still requires power to operate. The power produced by the SP can be stored in batteries during the day and used later during eclipse. Off the shelf batteries [20] for 1U, 3U and 6U CubeSats have the energy capacity of 19.24 Wh, 38.5 Wh and 77 Wh respectively. Typically the satellite power is divided evenly between the critical subsystems: housekeeping get 33 %, EP system get 33 % and the payload get 33 %.

2.4. Orbital constraints

Atmospheric drag is a major perturbation in LEO, despite the fact that CubeSats have a relatively small cross-sectional area. In orbits lower then 500 km the drag force overcomes the thrust magnitude of an EP thruster. To simplify the discussion, in this paper we assume at least one order of magnitude difference between the EP thrust and drag forces, and therefore limit the orbit height to be higher then 600 km.

Inter-satellite communication is crucial for mission success because of the need to share information between the cluster agents. Link budget analysis [21] show that inter-satellite communication is affected by many parameters such as: ISD, required data rate, transmission power and etc. Here we assume an ISD upper bound of 1000 km.

3. VERY LOW THRUST ORBIT CONTROL

3.1. Control law

Control law design have great impact on the cluster performance and different control approaches add different mission constraints [22]. Due to the limited computational power and limited communication capabilities we chose to focus on the cyclic approach [23]. This approach have the following benefits:

1. Limited information requirements - each agent interacts only with his nearest neighbor.
2. Robust - failed spacecraft do not affect the stability of the formation.
3. Scalable - the amount of agents can be increased without modifying the control law.
4. Decentralized and distributed - all agents are equal with respect to control, and there is no need of leader agents.

The controller goal is to limit the ISD drift by changing the mean semimajor axis (SMA). The controller use mean orbital elements as feedback. In this study orbital elements are organized in the following way:

$$\mathbf{E} = [a, e, i, \Omega, \omega, f]^T \tag{1}$$

Where a is the SMA, e is the eccentricity, h is the angular momentum, μ is the gravitational constant, i denotes the inclination, Ω denotes the right ascension of the ascending node, ω is the argument of perigee, f is the true anomaly, λ is the argument of latitude and $p \triangleq a(1-e^2)$. The mean orbital elements are obtained by the single averaging operator [24]:

$$\bar{\alpha} \triangleq \frac{1}{2\pi}\int_0^{2\pi} \alpha \mathrm{d}M \tag{2}$$

where α is the orbital element, $\bar{\alpha}$ is the mean orbital element and M is the mean anomaly. The controller is given by:

$$T_i = \begin{cases} 0 & \Delta\bar{a}_{ij}\Delta\bar{\lambda}_{ij} \geq 0 \\ -T_{max} sign\left(\Delta\bar{a}_{ij}\right) & \Delta\bar{a}_{ij}\Delta\bar{\lambda}_{ij} < 0 \end{cases} \qquad j = \begin{cases} i+1 & i = 1,2,3...N-1 \\ 1 & i = N \end{cases} \tag{3}$$

Where T is a thrust command in the in-track direction, T_{max} is the maximum thrust, $\bar{\lambda} = \bar{f} + \bar{\omega}$, $\Delta\bar{a}_{ij} \triangleq \bar{a}_i - \bar{a}_j$ and $\Delta\bar{\lambda}_{ij} \triangleq \bar{\lambda}_i - \bar{\lambda}_j$. The proposed controller is simple to implement on real time systems and can be done autonomously. The amount of required information is limited to $\Delta\bar{a}$ and $\Delta\bar{\lambda}$ of the j^{th} agent. The controller is using the neutral drift of the satellite to reduce fuel consumption. It is decentralized and can be adapted to a changing number of agent in the cluster.

3.2. Analytical model of the formation keeping maneuver

A CubeSat cluster is usually deployed from a single launcher, and is injected into the same orbit plane. The major difference between the CubeSats is their SMA. Lets consider a simple scenario [25] where two satellites are injected into near circular LEO ($e \ll 1$) with some SMA difference. The satellite will be subjected mainly to drag and J2 perturbations. We consider an analytical model that predicts the along track distance evolving over a few days of the cluster establishment maneuver. Although the model neglects J2 and drag perturbations, it is useful for determining the required thrust in order to maintain the ISD below maximal values for a short duration maneuver (less than 10 days) at specific initial conditions. We assume that the chief can maneuver and the deputy is cruising in a nominal orbit ($_C$ and $_D$ are chief and deputy respectably). If $\Delta\bar{a}_{CD}\Delta\bar{\lambda}_{CD} < 0$ at the initial time of deployment when $\Delta\bar{a}_{CD}\Delta\bar{\lambda}_{CD} = 0$ the couple will reach their maximum along track distance. This will happened when the chief and deputy SMA will be equal. To calculate the time a_C and a_D converged we use the Gauss variational equations (Appendix A.1) and replace the tangential acceleration with the acceleration created by the thrusters:

$$\dot{a} = \frac{da}{dt} = \frac{2a^2 v}{\mu}\frac{T_{max}}{m} \tag{4}$$

Integrating Eq. (4) over a gives us $\Delta t_{a_i \to a_f}$, the time from orbit injection till the maximal distance reached

$$\Delta t_{a_i \to a_f} = \frac{m\sqrt{\mu}}{2T}\int_{a_i}^{a_f}\frac{1}{\sqrt{a^3}}da = \frac{m\sqrt{\mu}}{T}\left[\frac{1}{\sqrt{a_i}} - \frac{1}{\sqrt{a_f}}\right] \tag{5}$$

Under the assumption of $e \ll 1$

$$\dot{\lambda} = \dot{f} + \dot{\omega} \approx \dot{M} + \dot{\omega} = n \tag{6}$$

The angular distance between the chief and the deputy at the end of the maneuver

$$\Delta\theta = \int_{t_i}^{t_f}\left(\dot{\lambda}_C - \dot{\lambda}_D\right)dt = \int_{t_i}^{t_f}\left(\sqrt{\frac{\mu}{a_C^3}} - \sqrt{\frac{\mu}{a_D^3}}\right)dt \tag{7}$$

The angular distance covered by the chief is given by

$$\Delta\theta_C = \int_{a_i}^{a_f}\left(\sqrt{\frac{\mu}{a_C^3}}\right)\frac{dt}{da}da = \frac{\mu m}{4T}\left(\frac{1}{a_i^2} - \frac{1}{a_f^2}\right) \tag{8}$$

And the angular distance covered by the uncontrolled deputy

$$\Delta\theta_D = \int_{t_i}^{t_f}\left(\sqrt{\frac{\mu}{a_D^3}}\right)dt = \sqrt{\frac{\mu}{a_D^3}}\Delta t_{a_i \to a_f} \tag{9}$$

We put Eq. (8) and Eq. (9) into Eq. (7) to obtain:

$$\Delta\theta_{a_C=a_D} = \frac{\mu m}{4T}\left(\frac{1}{a_i^2} - \frac{4}{\sqrt{a_i a_f^3}} + \frac{3}{a_f^2}\right) \tag{10}$$

Using the cosine law we obtain the along track distance:

$$d_{CD} = \sqrt{2}a_f\sqrt{1 - \cos\left(\Delta\theta_{a_C=a_D}\right)}\cos\frac{\Delta\theta_{a_C=a_D}}{2} \tag{11}$$

Table 2 shows the model result for different thrust values assuming two 6U CubeSats with mass of 8 kg, SMA of 7000 km and $\Delta a_{CD} = 1$ km.

Table 2. Inter - satellite distances example

$\mathbf{T}\,[\mu N]$	$\Delta t_{a_i \to a_f}\,[day]$	$d_{CD}\,[km]$
10	5	348
50	1	70
100	0.5	35

4. ALGORITHMS AND CONTROL METHODS

If one considers a non-constrained case where the satellite can re-orientate its thrust to any required direction this case will ensure an ideal performance of the above controller in terms of fuel consumption, converges in time and maximal ISD. However in a real power constrained mission, using thrusters can cause the battery to reach high depth of discharge (DOD) values. Also, it means that cluster keeping is the satellite first priority mission. Satellites usually set their housekeeping activities and payload activations as first and second priority. This means that thrusters can not be pointed to the required direction at all time and the cluster keeping performance might be affected. Here we describe four different approaches to cope with the mention conflicts. The first two methods are based on a time division method and offer a way to trade DOD values for maximal ISD and vice versa. The later two methods utilize the concept of allowed error cones and offer a way to preform successful cluster keeping while doing other high priority operation.

4.1. Fixed time slots method

One option to reduce the DOD values is to allow the satellite to preform maneuvers only during the umbra. In LEO orbital night are about $\frac{1}{3}$ of the satellite period. To compensate for the fact that electricity is not generated during the umbra we are dedicating the satellite attitude to collect solar power during the day. Table 3 shows the attitude requirement of this method. By limiting the thrust maneuvers to the night time

we reduce 66 % of the available control time compared to unconstricted case. Using the analytical model in section 3.2 we can predict that the maximal ISD will increase by factor for 3, proportional to $\frac{1}{\text{Duty cycle}}$.

We can split the satellite period to allocate several slots, dedicating a slot for payload operation. Adding more slots will reduce the amount of time spent on each slot and can reduce the power generated, increase the maximal ISD and increase the fuel consumption. Such a time division method is easy to implement and promise to fulfill a hard constraint on each of the required operation slots.

Table 3. Attitude requirements for the fixed time slots and cosine methods

Night	Day
$x_{\mathcal{B}} = \mathbf{T}$	$z_{\mathcal{B}} = \mathbf{s}$
$y_{\mathcal{B}} = \mathbf{T} \times \mathbf{s}$	$y_{\mathcal{B}} = \mathbf{s} \times \mathbf{v}$
$z_{\mathcal{B}} = y_{\mathcal{B}} \times x_{\mathcal{B}}$	$x_{\mathcal{B}} = y_{\mathcal{B}} \times z_{\mathcal{B}}$

4.2. Dynamic time slots method

We can consider a different time division approach where the time slots are based on data collected in real time. Fig. 3 shows an activity diagram of this method. Upper and lower bounds should be set in advance by the designer to meet the lifetime requirement of the satellite. We can use the same concept and add the nadir point mode. Fig. 4 shows an activity diagram of the proposed method. In this example the nadir pointing mode have a priority over the orbit control mode. Like the above example, this method will ensure bounded DOD values and the payload / EP will only be activated when the DOD status is nominal.

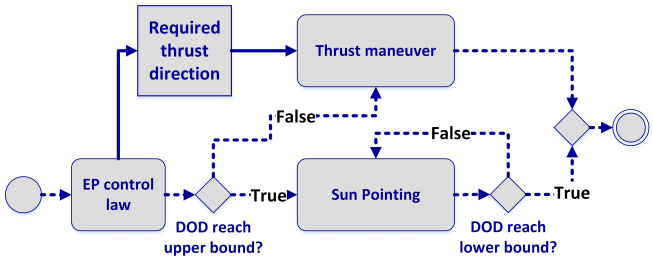

Fig. 3. DOD method activity diagram

4.3. Cosine Method

SP maximum power is reached when the SPs axis $\hat{\mathbf{z}}_{\mathcal{B}}$ is aligned with the sun vector $\hat{\mathbf{s}}$. The remaining DOF can be used to bring the thrust vector $\hat{\mathbf{x}}_{\mathcal{B}}$ as close as possible to the velocity vector $\hat{\mathbf{v}}$. Using the thruster while the thrust vector is not pointed into the right direction might cause problems,

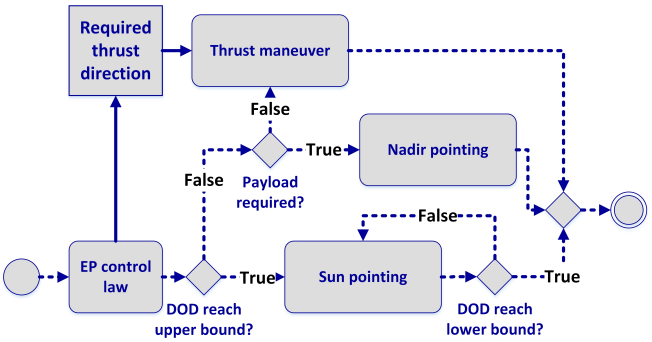

Fig. 4. DOD method with nadir pointing payload activity diagram

such as excessive use of fuel and creating unwanted differences in the orbital elements. The analysis presented in appendix A.2 shows that even 20° misalignment will have very small affect on the cluster keeping performance. Instead of having a strict attitude constraint that allows us to fire only when $\hat{\mathbf{x}}_{\mathcal{B}} \cdot \hat{\mathbf{v}} = 1$ we can now fire when $\hat{\mathbf{x}}_{\mathcal{B}} \cdot \hat{\mathbf{v}} \geq \cos 20°$ without creating too much unwanted effect in the orbital elements. Fig. 5 shows an activity diagram utilising this concept and Table 3 shows the attitude requirement of this method. During umbra the satellite preform precise thrust maneuvers and during the day the satellite points towards the sun and preform thrust maneuver only when $\hat{\mathbf{x}}_{\mathcal{B}} \cdot \hat{\mathbf{v}} \geq \cos 20°$. Using this method we ensure maximal power generation while preforming limited cluster control. We term it the cosine method due to the allowed error cone around the velocity vector.

4.4. Double Cosine Method

The cosine method have one hard constraint and one soft constraint. If we can tolerate some error in our sun pointing accuracy the sun pointing hard constraint can be modified to a soft constraint. The satellite attitude affect on the power production is modeled by

$$P_{sp} = P_{sp_0} cos\theta_s \tag{12}$$

where P_{sp} is the power produce by the SP, P_{sp_0} is the SP nominal power and θ_s is the sun incidence angle. This cosine law holds only for sun angles between $0° - 50°$. For more accurate results a Kelly cosine can be used [26]. Eq. (12) shows that pointing the solar panels with 20° error will only reduce the generated power by 6 %. The new soft constraint creates an additional DOF. The new DOF can be used to maximize the thrust time while keeping the DOD values low. We define ϵ_p as the allowed error between $\hat{\mathbf{z}}_{\boldsymbol{\mathcal{B}}}$ and $\hat{\mathbf{s}}$ and ϵ_t as the allowed error between $\hat{\mathbf{x}}_{\boldsymbol{\mathcal{B}}}$ and $\hat{\mathbf{v}}$.

These allowed errors create two cones hance this method is termed here as the double cosine method. We can calculate the separation angle between $\hat{\mathbf{s}}$ and $\hat{\mathbf{v}}$

$$\cos(\theta) = \hat{\mathbf{s}} \cdot \hat{\mathbf{v}} \tag{13}$$

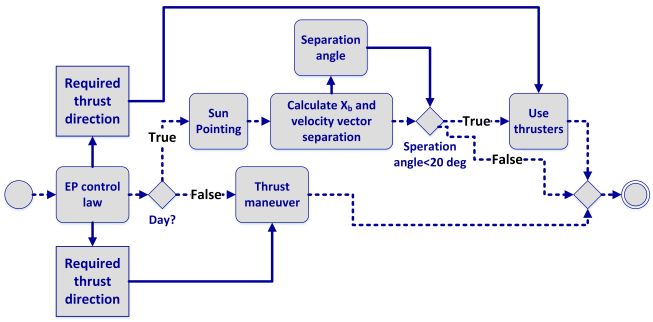

Fig. 5. Cosine method activity diagram

We can use the $\hat{\mathbf{s}}$ and $\hat{\mathbf{v}}$ plane to create the NSW frame ($\mathcal{N}_s$) presented in Fig. 6(a) where

$$N = \hat{\mathbf{s}} \times \hat{\mathbf{v}}, \quad W = (\hat{\mathbf{s}} \times \hat{\mathbf{v}}) \times \hat{\mathbf{s}}, \quad S = \hat{\mathbf{s}} \tag{14}$$

The projection of $\hat{\mathbf{v}}_{\mathcal{I}}$ on the $\mathcal{N}_s$ frame is:

$$\hat{\mathbf{v}}_{\mathcal{N}_s} = D^{\mathcal{I}}_{\mathcal{N}_s} \hat{\mathbf{v}}_{\mathcal{I}} = [0, v_y, v_z] \tag{15}$$

where $D^{\mathcal{I}}_{\mathcal{N}_s}$ is the direction cosine matrix (DCM) that rotates vectors from $\mathcal{I}$ frame to the $\mathcal{N}_s$ frame. The projection of $\hat{\mathbf{z}}_{\mathcal{B}}$ on the $\mathcal{N}_s$ frame is:

$$\hat{\mathbf{z}}_{\mathcal{B}\mathcal{N}_s} = \begin{bmatrix} \cos\alpha\cos\delta & \sin\alpha\cos\delta & \sin\delta \end{bmatrix} \tag{16}$$

where the right ascension, denoted by $\alpha \in [0, 2\pi)$ and the declination, denoted by $\delta \in \left[-\frac{\pi}{2}, \frac{\pi}{2}\right)$. The projection of $\hat{\mathbf{x}}_{\mathcal{B}}$ on the $\mathcal{N}_s$ frame is:

$$\hat{\mathbf{x}}_{\mathcal{B}\mathcal{N}_s} = \begin{bmatrix} \cos\alpha\sin\delta & \sin\alpha\sin\delta & -\cos\delta \end{bmatrix} \tag{17}$$

Now we can calculate ξ, the separation angle between $\hat{\mathbf{x}}_{\mathcal{B}\mathcal{N}_s}$ and $\hat{\mathbf{v}}_{\mathcal{N}_s}$

$$\cos(\xi) = \hat{\mathbf{x}}_{\mathcal{B}\mathcal{N}_s} \cdot \hat{\mathbf{v}}_{\mathcal{N}_s} = (\sin\alpha\sin\delta)\, v_y - (\cos\delta)\, v_z \tag{18}$$

Our goal in this method is to minimize $|\xi|$ while

$$\hat{\mathbf{z}}_{\mathcal{B}\mathcal{N}_s} \cdot \hat{\mathbf{s}}_{\mathcal{N}_s} \geq \cos\epsilon_p \tag{19a}$$
$$\hat{\mathbf{x}}_{\mathcal{B}\mathcal{N}_s} \cdot \hat{\mathbf{v}}_{\mathcal{N}_s} \geq \cos\epsilon_t \tag{19b}$$

Fig. 6(b) shows that this method is only effective when

$$\left(\frac{\pi}{2} - 2\epsilon_{pt}\right) < \theta < \left(\frac{\pi}{2} + 2\epsilon_{pt}\right) \tag{20}$$

where $\epsilon_{pt} = min(\epsilon_p, \epsilon_t)$. We can find α and δ that minimize $|\xi|$ by deriving Eq. (18) and look for the maximum values.

$$\begin{aligned} \frac{df(\alpha,\delta)}{d\alpha} &= (\cos\alpha\sin\delta)\, v_y \\ \frac{d^2 f(\alpha,\delta)}{d\alpha^2} &= (-\sin\alpha\sin\delta)\, v_y \end{aligned} \tag{21}$$

From Eq. (21) we see that if $\sin\delta v_y > 0$ then the maximum can be found at $\alpha = \frac{\pi}{2}$ and if $\sin\delta v_y < 0$ then the maximum can be found at $\alpha = -\frac{\pi}{2}$. Deriving Eq. (18) again this time by δ

$$\begin{aligned} \frac{df(\alpha,\delta)}{d\delta} &= (\sin\alpha\cos\delta)\, v_y + (\sin\delta)\, v_z \\ \delta &= \tan^{-1}\left(-\sin\alpha\frac{v_y}{v_z}\right) \\ \frac{d^2 f(\alpha,\delta)}{d\delta^2} &= \cos\delta\left(\frac{\sin^2\alpha v_y^2}{v_z} + v_z\right) \end{aligned} \tag{22}$$

From Eq. (22) we see that if $v_z < 0$ then we obtain the maximum value when $\delta > 0$ and if $v_z > 0$ we obtain the maximum when $\delta < 0$. Now we should rotate the required direction for z_b from the $\mathcal{N}_s$ frame back to $\mathcal{I}$ using $D^{\mathcal{N}_s}_{\mathcal{I}}$ and the required attitude can be described by the following equation:

$$\mathbf{z_b} = D^{\mathcal{N}_s}_{\mathcal{I}} \mathbf{z_{b_{\mathcal{N}_s}}}, \quad \mathbf{y_b} = \mathbf{z_b} \times \mathbf{v}, \quad \mathbf{x_b} = \mathbf{y_b} \times \mathbf{z_b} \tag{23}$$

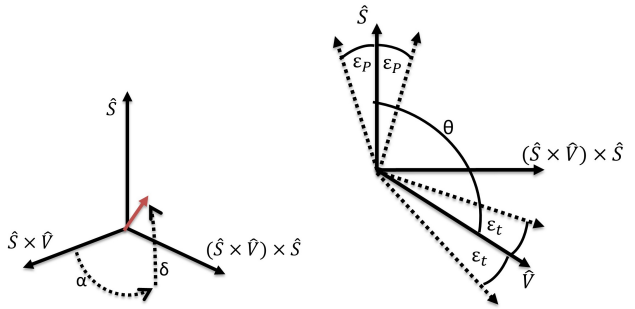

(a) NSW frame where N point towards $\hat{\mathbf{s}} \times \hat{\mathbf{v}}$ and S point towards $\hat{\mathbf{s}}$

(b) SW plane of the NSW frame including the error cones around $\hat{\mathbf{s}}$ and $\hat{\mathbf{v}}$ and the separation angle θ

Fig. 6. NSW frame

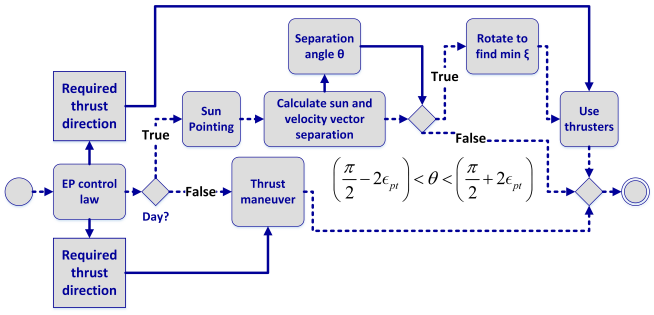

Fig. 7. Double cosine method activity diagram

5. RESULTS AND DISCUSSION

5.1. Numerical simulation setup

Several simulation were preformed to test the methods developed in section 4. The FreeFlyer software [27] was used as a high fidelity orbit propagator that includes a drag model, a solar radiation pressure model, earth zonal and tesseral potential terms, the moon's gravity field and the sun's gravity

field. FreeFlyer was also used to implement the closed loop controller and satellite logic using the built-in tools.

5.1.1. *Electric power system modelling*

We introduce to the orbital simulation a simplified electric power system model that consider only a power source and energy storage components. In this work we model the affect of satellite attitude on the electric power system while assuming a constant electrical efficiency of the system. Each of the satellite sub-systems requires power and combining all of them together gives us P_l. Integrating P_{sp} and P_l over time gives the generated energy E_{sp} and the required energy E_l. The relation between the energy produced by the SP E_{sp}, the energy consumed by the loads E_l, and the battery energy E_b is given by:

$$E_b(t) = E_b(t-1) + E_{sp} - E_l \tag{24}$$

Battery charge and discharge rates are measured as a fraction of the rated energy $E_b(0)$. The DOD affects the battery performance (for example cell voltage, battery lifetime). The DOD and the state of charge (SOC) are calculated by :

$$SOC = \frac{E_b(t)}{E_b(0)} = 1 - DOD \tag{25}$$

Calculating the sun incidence angle θ_s can be obtain by

$$\theta_s = \cos^{-1}\left(\hat{\mathbf{n}}_{sp_{\mathcal{B}}} \cdot \hat{\mathbf{s}}_{\mathcal{B}}\right) \tag{26}$$

where $\hat{\mathbf{s}}_{\mathcal{B}}$ is the normalized sun vector in $\mathcal{B}$ and $\hat{\mathbf{n}}_{sp_{\mathcal{B}}}$ is the normal to the solar panel surface in $\mathcal{B}$. In general case, where the satellite's shape is unknown, this calculation might be more complex due to the effect of surface shadow [28]. In the case of CubeSats with DSP pointed to the same direction the shadow effect vanish.

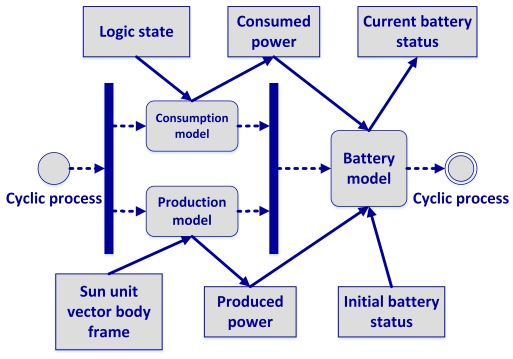

Fig. 8. electric power system simulation activity diagram

5.2. Case study

As a case study we assume a cluster of 3 6U CubeSats. The 6U physical and electrical power constraints are described in Table 1. The CubeSat thruster create 100 μN with I_{sp} of 1000 s. Figure 2 shows the body frame of the above configuration. Consider a local vertical local horizontal (LVLH) rotating coordinate system in which $Z_{\mathcal{L}}$ points along the radial direction, $Y_{\mathcal{L}}$ along the orbit normal and $X_{\mathcal{L}}$ completing the system. In the chosen example the cluster orbit injection procedure and initial conditions are defined in [29]. The satellites are released one by one with constant time difference between them. The release velocity Δv created by the P-Pod is set to be $\Delta v = 2\frac{\text{m}}{\text{s}}$. The first CubeSat launch towards the $Z_{\mathcal{L}}$. The second CubeSat is released after $\Delta t = 35$ s while the launcher preforms 30° maneuver around the $Y_{\mathcal{L}}$. The third satellite is released 70 s after the first one while the launcher preforms another 30° maneuver around $Y_{\mathcal{L}}$. Launcher orbit elements at the release of the first satellite are:

$$\mathbf{E_0} = [7000,\ 0,\ 63°,\ 0°,\ 0°,\ 0°]^T \tag{27}$$

These initial conditions were used for all the simulation sessions.

5.3. Non constrained performance

To create a reference to the other methods we test the ideal performance of the controller. The non constrained case assumes that the satellite can thrust in the required direction whenever needed. We assume that the satellite attitude is changing according to the algorithm presented in Table 4. We can use the satellite orientation to calculate DOD values using the electric power system model simulation presented in Section 5.1.1. For the non constrained case the maximal ISD is 196 km (Fig. 9(a)), the controller coverage after 5 days and fuel consumption is 1.26 g. Fig. 9(b) shows a full year simulation of this case. The problem in this result is that after less then a day DOD values reach 100 % meaning that in a real scenario the satellite will not have enough power to operate.

Table 4. Non constrained case - attitude requirements

Thrust required	No thrust reuired
$x_{\mathcal{B}} = \mathbf{T}$	$z_{\mathcal{B}} = \mathbf{s}$
$y_{\mathcal{B}} = \mathbf{T} \times \mathbf{s}$	$y_{\mathcal{B}} = \mathbf{s} \times \mathbf{v}$
$z_{\mathcal{B}} = y_{\mathcal{B}} \times x_{\mathcal{B}}$	$x_{\mathcal{B}} = y_{\mathcal{B}} \times z_{\mathcal{B}}$

5.4. Time division methods performance

The first time division method (Section 4.1) assumes that the thruster can be activated only during the night while the satellite charges its batteries during the day. For this case the maximal ISD is 591 km, the controller coverage after 14.8 days, fuel consumption is 1.35 g and maximal DOD is 20 % (See Fig. 10). Here we see an agreement with the analytical model as the ISD increased by a factor of 3 compared to the non

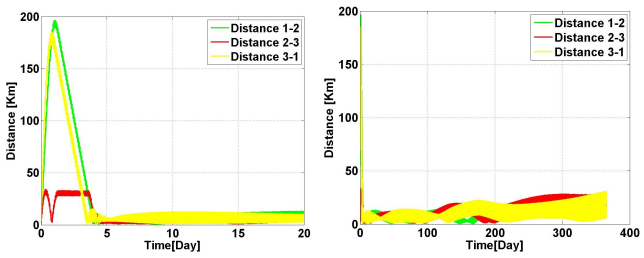

(a) First 20 days (b) Full year simulation

Fig. 9. Non constrained performance - ISD result

constrained case. The maximal DOD value is lower relative to the non constrained method.

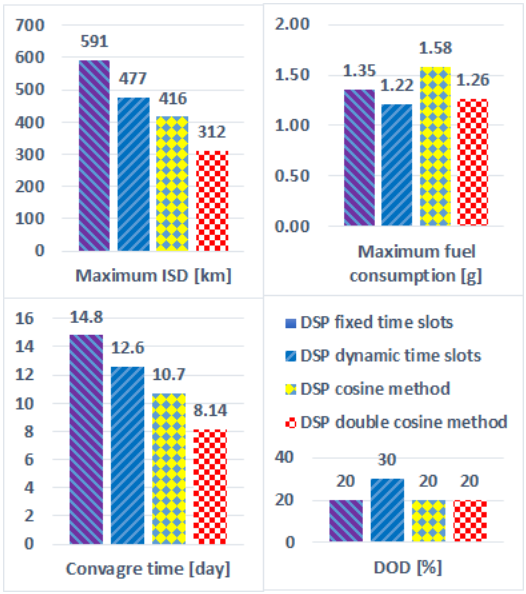

Fig. 10. Time division and cosine methods - result summary

To improve the performance we can consider a second time division method where the time slots are set based on real time collected data. The second time division method (Section 4.2) uses DOD measurements to decided if a thruster can be activated. For this simulation the DOD upper bound was set to 20 % and the lower bound is 10 %. For this case the maximal ISD is 477 km, the controller coverage after 12.6 days, fuel consumption is 1.22 g and the maximal DOD is 30 %. In this method we are able to exchange higher DOD values for lower ISD.

To estimate the control effort of the above methods we can assume that the control effort is proportional to the required angular rate. Fig. 11(a) shows the angular rate of a satellite when its orientation is dedicated to sun-pointing. Fig. 11(b) shows the case where the satellite point its thrusters to the velocity direction. The peaks occur when the satellite enters or leaves the area of sun exposure. The required attitude can be found in Table 3. In both cases the required angular rate is below $1\frac{\text{deg}}{\text{s}}$ at all time. We note that moving from one pointing mode to another might take time considering the angular separation between the current state and the required one.

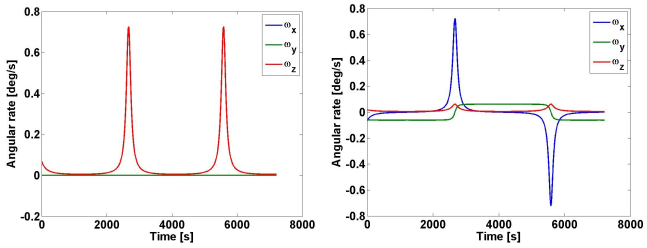

(a) Sun pointing mode (b) Thrust mode

Fig. 11. Satellite angular rate in different pointing modes

5.5. Cosine methods performance

The cosine method assumes that the satellite points its SP towards the sun during the day while minimizing the separation angle between $\hat{\mathbf{x}}_{\mathcal{B}}$ and $\hat{\mathbf{v}}$ (Section 4.3). During the night the satellite can activate its thrusters with no limitation. In this simulation the allowed error is 20°. A numerical simulation of this method show that the maximal ISD is 416 km, the controller coverage after 10.7 days, fuel consumption is 1.58 g and maximal DOD is 20 % (Fig. 10). In Fig. 12 we show the benefits of the double cosine method compared to the cosine method. Data is shown only for the day section of the orbit. Fig. 12(a) shows the separation angle between $\hat{\mathbf{s}}$ and $\hat{\mathbf{v}}$ (solid line) and the area where this method can be activated (bounded by the dashed lines). For these initial conditions roughly 0.5 of the day time can be dedicated for thrust maneuver. Fig. 12(b) shows the separation angle between $\hat{\mathbf{x}}_{\mathcal{B}}$ and $\hat{\mathbf{v}}$ where the diamonds represent the cosine method, the circles represent the double cosine method and the solid lines represent the allowed thrust zone. We see that using this method we can increase the day thrust time by a factor of 3 compared to the cosine method. Another benefit of using the double cosine method is that for a large section of the thrusting time we can fire directly in $\hat{\mathbf{v}}$ direction. In this example we have 6000 s period with 4000 s daytime then using the cosine method we can apply thrust on $\sim$ 45 % of the period. With the double cosine method we can apply $\sim$ 65 %. Using the analytic model (Section 3.2) we can predict that the cosine method ISD will be 2.2 time larger then the non constrained method. Using the same model with the double cosine method the ISD will increase by 1.54. The numerical simulation of this method show that the maximal ISD is 312 km, the controller coverage after 8.2 days, fuel consumption is 1.26 g and maximal DOD is 20 % (Fig 10). The ISD increased by a factor of 2.1 and 1.59 for the cosine and double cosine methods respectively compared to the non constrained case. Fig. 13(a) shows the angular rate of the satellite when

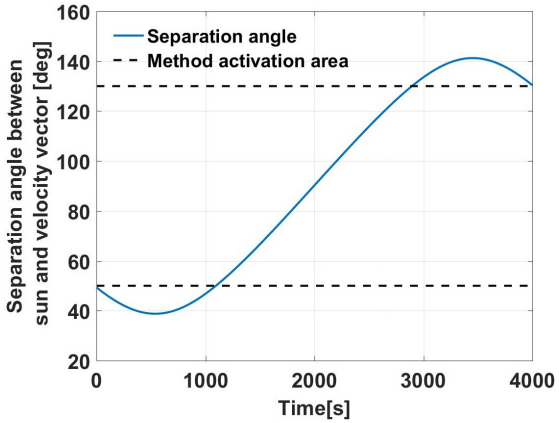

(a) Separation between $\mathbf{s}$ and $\mathbf{v}$

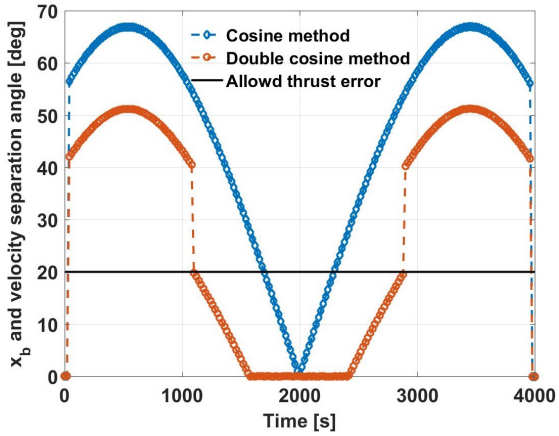

(b) Separation between $\mathbf{x_b}$ and $\mathbf{v}$

Fig. 12. Comparison between cosine and double cosine methods

executing the cosine method. The required attitude for the cosine mode can be found in Table 3. The black dashed lines mark the transient maneuver with $0.25\ \frac{\text{deg}}{\text{s}}$ angular rate limit. The duration of the transient maneuver can be lower if we increase the angular rate limit. The peaks in the angular rate of the sun pointing mode occurs when the satellite enters or leaves the direct sun area. To the right of the dashed lines we see the angular rate of the thrust mode. Fig. 13(b) shows the angular rate of a satellite when executing the double cosine method, in this case we present only the day time. The two green peaks occur when $\hat{\mathbf{z}}_{\mathcal{B}}$ jumps from the sun vector to the edge of the cone. Between the two peaks an area of constant angular rate is present where $\hat{\mathbf{x}}_{\mathcal{B}}$ is pointed to $\hat{\mathbf{v}}$ and $\hat{\mathbf{z}}_{\mathcal{B}}$ is traveling through the cone. In both cases the required angular rate is below $1\ \frac{\text{deg}}{\text{s}}$.

6. CONCLUSIONS

Analysis of CubeSats typical constraints indicates four major constraints: structure, attitude, electric power and orbit. Following these constraints, a cyclic controller was developed based on a low-power EP system. The controller modifies the CubeSats SMA according to their relative position with respect to the closest satellite in the formation. An EP system offers a challenge to the CubeSat electric power and attitude subsystems. To operate the EP system four method were developed. Two time division methods allocate dedicated time slots for each of the satellite main tasks, fulfill one hard constraint at a time. Two cosine methods define an error cone around the required orientation that allows the satellite to fulfill two soft constraints in parallel. A high fidelity orbit simulations was used to test these methods. A test case of 3 6U CubeSats cluster deployed from a single launcher with 100 μN thruster was chosen. The simulation results show that all methods were able to eliminate the drift with less than 2 g of fuel within less then 20 days after the orbit injection. The lowest ISD was achieved using the double cosine method. During the maneuver the satellites can maintain first priority tasks while the orbit control operate as second priority. An analysis was done to estimate the attitude system control effort by monitoring the satellite angular rate, validating the feasibility of these methods with low power attitude actuators. An electric power system simulation module were used to monitor CubeSat power production, storage and consumption validating the feasibility of these methods with real power constraints. To conclude, it was demonstrated that the proposed methods presented here enable to maintain a realistic CubeSat formation flying mission using low power EP.

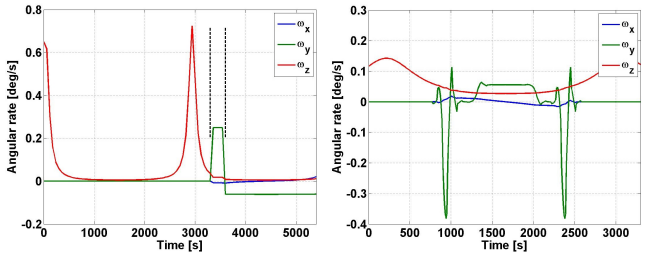

(a) Cosine method (b) Double cosine method

Fig. 13. Satellite angular rate in cosine and double cosine modes

Acknowledgment

E.E would like to acknowledge fruitful discussion with Pini Gurfil and Ohad Ben-Yaakov from the Distributed Space Systems Laboratory.

7. REFERENCES

[1] Kyle Alfriend, Srinivas Rao Vadali, Pini Gurfil, Jonathan How, and Louis Breger, *Spacecraft Forma-*

tion Flying: Dynamics, Control and Navigation, vol. 2, Butterworth-Heinemann, 2009.

[2] Marco D'Errico, *Distributed Space Missions for Earth System Monitoring*, vol. 31, Springer Science & Business Media, 2012.

[3] David J Barnhart, Tanya Vladimirova, and Martin N Sweeting, "Very-small-satellite design for distributed space missions," *Journal of Spacecraft and Rockets*, vol. 44, no. 6, pp. 1294–1306, 2007.

[4] Simone D'Amico, Jean-Sebastien Ardaens, and Sergio De Florio, "Autonomous formation flying based on gps prisma flight results," *Acta Astronautica*, vol. 82, no. 1, pp. 69–79, 2013.

[5] Eberhard Gill, Oliver Montenbruck, and Simone D'Amico, "Autonomous formation flying for the prisma mission," *Journal of Spacecraft and Rockets*, vol. 44, no. 3, pp. 671–681, 2007.

[6] Grant Bonin, Niels Roth, Scott Armitage, Josh Newman, Ben Risi, and Robert E Zee, "Canx–4 and canx–5 precision formation flight: Mission accomplished!," 2015.

[7] P. Gurfil, J. Herscovitz, and M. Pariente, "The samson project - cluster flight and geolocation with three autonomous nano-satellites," in *26th AIAA/USU Conference on Small Satellites*, 2012.

[8] Leonel Mazal and Pini Gurfil, "Closed-loop distance-keeping for long-term satellite cluster flight," *Acta Astronautica*, vol. 94, no. 1, pp. 73–82, 2014.

[9] Dan R Lev, Jacob Herscovitz, Zvi Zuckerman, Zeev Dvorkin, Daniel Kariv, Itzhak Mizrachi, and Hadar Ricardo, "Cold gas propulsion system conceptual design for the samson nano-satellite," in *50th AIAA/ASME/SAE/ASEE Joint Propulsion Conference*, 2014.

[10] Ryan W Conversano and Richard E Wirz, "Mission capability assessment of cubesats using a miniature ion thruster," *Journal of Spacecraft and Rockets*, vol. 50, no. 5, pp. 1035–1046, 2013.

[11] Igal Kronhaus, Klaus Schilling, Mathias Pietzka, and Jochen Schein, "Simple orbit and attitude control using vacuum arc thrusters for picosatellites," *Journal of Spacecraft and Rockets*, vol. 51, no. 6, pp. 2008–2015, 2014.

[12] Nikolaos A Gatsonis, Ye Lu, John J Blandino, Michael A Demetriou, and Nicholas Paschalidis, "Micro pulsed plasma thrusters for attitude control of a low earth orbiting cubesat," *submitted June 2015 to the AIAA Journal of Spacecraft and Rockets, in review*, 2016.

[13] Juergen Mueller, Richard Hofer, and John Ziemer, "Survey of propulsion technologies applicable to cubesats," *Jet Propulsion Laboratory*, 2010.

[14] Michael Keidar, Taisen Zhuang, Alexey Shashurin, George Teel, Dereck Chiu, Joseph Lukas, Samudra Haque, and Lubos Brieda, "Electric propulsion for small satellites," *Plasma Physics and Controlled Fusion*, vol. 57, no. 1, pp. 014005, 2015.

[15] A Ruggiero, P Pergola, S Marcuccio, and M Andrenucci, "Low-thrust maneuvers for the efficient correction of orbital elements," in *32nd International Electric Propulsion Conference*, 2011, pp. 1–13.

[16] Hank Heidt, Jordi Puig-Suari, Augustus Moore, Shinichi Nakasuka, and Robert Twiggs, "Cubesat: A new generation of picosatellite for education and industry low-cost space experimentation," in *Proceedings of the 14th Annual/USU Conference on Small Satellites, Logan, USA*, 2000.

[17] Simon Lee, Amy Hutputanasin, Armen Toorian, Wenschel Lan, and R Munakata, "Cubesat design specification rev. 13," *The CubeSat Program*, 2015.

[18] Shailesh Notani and Subhashish Bhattacharya, "Flexible electrical power system controller design and battery integration for 1u to 12u cubesats," in *Energy Conversion Congress and Exposition (ECCE), 2011 IEEE*. IEEE, 2011, pp. 3633–3640.

[19] Fabio Santoni, Fabrizio Piergentili, Serena Donati, Massimo Perelli, Andrea Negri, and Michele Marino, "An innovative deployable solar panel system for cubesats," *Acta Astronautica*, vol. 95, pp. 210–217, 2014.

[20] GOMSPACE, "http://gomspace.com/index.php?p=products-power," .

[21] Wiley J Larson and James Richard Wertz, "Space mission analysis and design," Tech. Rep., Microcosm, Inc., Torrance, CA (US), 1992.

[22] Daniel P Scharf, Fred Y Hadaegh, and Scott R Ploen, "A survey of spacecraft formation flying guidance and control. part ii: control," in *American Control Conference, 2004. Proceedings of the 2004*. IEEE, 2004, vol. 4, pp. 2976–2985.

[23] Ohad Ben-Yaacov and Pini Gurfil, "Stability and performance of orbital elements feedback for cluster keeping using differential drag," *The Journal of the Astronautical Sciences*, pp. 1–29, 2014.

[24] Dirk Brouwer, "Solution of the problem of artificial satellite theory without drag," *The Astronomical Journal*, vol. 64, pp. 378, 1959.

[25] Fernando Zimmerman, "Ppt assisted formation keeping o nanosatellites under j2 and drag," M.S. thesis, Technion, 2014.

[26] Mukund R Patel, *Spacecraft power systems*, CRC press, 2004.

[27] AI Solutions, "Freeflyer users guide," *AI Solutions, March*, 1999.

[28] Ohad Ben-Yaacov, Eviatar Edlerman, and Pini Gurfil, "Analytical technique for satellite projected cross-sectional area calculation," *Advances in Space Research*, 2015.

[29] Changxuan Wen, Hao Zhang, and Pini Gurfil, "Orbit injection considerations for cluster flight of nanosatellites," *Journal of Spacecraft and Rockets*, vol. 52, no. 1, pp. 196–208, 2014.

[30] R. H. Battin, *An Introduction to the Mathematics and Methods of Astrodynamics*, AIAA Education Series, 1987; Chapter 8, pp. 401-408; Chapter 10, pp. 495-508.

[31] Hassan K Khalil and JW Grizzle, *Nonlinear systems*, vol. 3, Prentice hall New Jersey, 1996.

A. APPENDIX

A.1. Gauss variational equations

The general nonlinear dynamics of a satellite under perturbations or control forces can be modeled using the Guass Variational Equations (GVEs). GVEs can be written in NTW frame ($\mathcal{N}_\mathcal{T}$) based on [30].

$$\frac{\mathrm{d}a}{\mathrm{d}t} = \left(\frac{2a^2v}{\mu}\right)u_t \tag{28a}$$

$$\frac{\mathrm{d}e}{\mathrm{d}t} = \left(\frac{2\left(e+\cos f\right)}{v}\right)u_t - \left(\frac{r}{av}\sin f\right)u_n \tag{28b}$$

$$\frac{\mathrm{d}i}{\mathrm{d}t} = \left(\frac{r\cos\lambda}{h}\right)u_w \tag{28c}$$

$$\frac{\mathrm{d}\omega}{\mathrm{d}t} = \left(\frac{2\sin f}{ev}\right)u_t + \left(\frac{2e+\frac{r}{a}\cos f}{ev}\right)u_n - \left(\frac{r\sin\lambda\cos i}{h\sin i}\right)u_w \tag{28d}$$

$$\frac{\mathrm{d}\Omega}{\mathrm{d}t} = \left(\frac{r\sin\lambda}{h\sin i}\right)u_w \tag{28e}$$

$$\frac{\mathrm{d}M}{\mathrm{d}t} = n - \left(\frac{2\sqrt{1-e^2}}{ev}\left(1+\frac{e^2r}{p}\right)\sin f\right)u_t - \left(\frac{r\sqrt{1-e^2}\cos f}{eav}\right)u_n \tag{28f}$$

The vector $\mathbf{u} = [u_t, u_n, u_w]^T$ represents acceleration written in $\mathcal{N}_\mathcal{T}$, where u_t, u_w and u_n are the velocity, orbit normal and the along radial acceleration respectively.

A.2. Sensitivity analysis of cluster performance to thrust errors

This section present and analysis that examined the affect of 20° misalignment from $\hat{\mathbf{v}}$ on each of the elements change rate, compered to the ideal performance. The analysis was carried out using the GVE equations Eq. (28) and under the assumption that thrust is the only perturbation. From Eq. (28a) we see that $\frac{\mathrm{d}a}{\mathrm{d}t}$ is affected only by the thrust component in the velocity direction. In the worst case $u_t = T_{max}\cos 20^\circ = 0.94T_{max}$ so $\frac{\mathrm{d}a}{\mathrm{d}t}$ has change only by 6 %. This might slightly increase the overall fuel consumption.

$$\Delta\frac{\mathrm{d}a}{\mathrm{d}t} = \frac{\left(\frac{2a^2v}{\mu}\right)0.94T_{max}}{\left(\frac{2a^2v}{\mu}\right)T_{max}} \tag{29}$$

We can approximate Eq. (28b) under near circular orbit assumption to be:

$$\frac{\mathrm{d}e}{\mathrm{d}t} \underset{e\ll 1}{\approx} \sqrt{\frac{a}{\mu}}\left(2u_t - u_n\right) \tag{30}$$

In the worst case these two components will combine so we will get:

$$\frac{\mathrm{d}e}{\mathrm{d}t} \approx 2.22\sqrt{\frac{a}{\mu}}\frac{T_{max}}{m} \tag{31}$$

Eq. (31) shows that the change from the ideal case is about 10%. We can approximate Eq. (28c) under near circular orbit assumption to be:

$$\frac{\mathrm{d}i}{\mathrm{d}t} \underset{e\ll 1}{\approx} 0.34T_{max}\sqrt{\frac{a}{\mu}} \tag{32}$$

Lets replace the parameters with real numbers of LEO satellite $a = 7000$ km with $100\,\mu$N thruster and mass of 8 kg. With these number the change in i over one day is about 0.0028°. We can approximate Eq. (28e) under near circular orbit assumption to be:

$$\frac{\mathrm{d}\Omega}{\mathrm{d}t} \underset{e\ll 1}{\approx} 0.34T_{max}\sqrt{\frac{a}{\mu}} \tag{33}$$

Replacing the parameters with similar parameters to the previous analysis will create a change in Ω that will accumulate over one day to be about 0.0028°. Using the circular orbit approximate is a bit problematic when talking on Eq. (28g) and Eq. (28e). These two equation have e in the denominator. We can rewrite Eq. (28g) as

$$\frac{\mathrm{d}M}{\mathrm{d}t} = n - Xu_t - Yu_n \tag{34}$$

Calculate $\frac{X}{Y}$ eliminate e in the denominator and if e is close to zero then this ratio is 2. In the ideal case the $\frac{\mathrm{d}M}{\mathrm{d}t}$ contribution due to thrust is equal to X and in the misalignment case this contribution is equal to $X\cos(20)+Y\sin(20)=X\cos(20)+\frac{X}{2}\sin(20)$. So the maximal change between the two cases is about 10%. If we set $e=0.01$ then Eq. (28e) can rewrite as:

$$\frac{\mathrm{d}\omega}{\mathrm{d}t}\approx\frac{2}{0.01v}u_t+\frac{1}{0.01v}u_n+\sqrt{\frac{a}{\mu}}u_w \tag{35}$$

Placing LEO parameters as before, the misalignment case shows about 10% difference from the ideal case. This analysis shows us that the performance difference between the ideal case and the 20° case over a short time period is negligible.

A.3. Stability proof of the cyclic controller

The controller in Eq. (3) can be reduce to depend on a single state $\Delta\bar{a}_{ij}$. The rate of change of the osculating λ is given by Eq. (28):

$$\dot{\lambda}=\dot{\omega}+\dot{M}=n-\dot{\Omega}\cos i \tag{36}$$

Under the assumption that the only perturbation is the thrust force, the mean argument of latitude is:

$$\dot{\bar{\lambda}}=\bar{n} \tag{37}$$

Hence,

$$\Delta\dot{\bar{\lambda}}_{ij}=\bar{n}_i-\bar{n}_j=\sqrt{\frac{\mu}{\bar{a}_i^3}}-\sqrt{\frac{\mu}{\bar{a}_j^3}} \tag{38}$$

Eq. (38) shows that if $\Delta\bar{a}_{ij}\to 0$ then $\bar{a}_i\approx\bar{a}_j$ and so $\Delta\dot{\bar{\lambda}}_{ij}\to 0$ and $\Delta\bar{\lambda}_{ij}\to const$ showing that $\Delta\bar{a}_{ij}$ is the controller's only state. To prove that the controller is an asymptotic stable in the sense that

$$\lim_{t\to\infty}\Delta\bar{a}\left(t\right)\to 0 \tag{39}$$

We use a Lyapunov function:

$$V=\frac{1}{2}\Delta a_{12}^2 \tag{40}$$

where V is continuously differentiable function. The closed-loop system is stable if the following conditions are satisfied:

$$V\left(\Delta\bar{a}\right)>0,\qquad\forall\Delta\bar{a}\neq 0 \tag{41a}$$

$$V\left(\Delta\bar{a}=0\right)=0 \tag{41b}$$

$$\dot{V}\left(\Delta\bar{a}\right)\leq 0 \tag{41c}$$

The system is asymptotically stable if:

$$\dot{V}\left(\Delta\bar{a}\right)<0,\qquad\forall\Delta\bar{a}\neq 0 \tag{41d}$$

The first two conditions Eq. (41a) and Eq. (41b) are automatically satisfied by Eq. (40). The third condition Eq. (41c) should be checked for the 4 cases of Eq. 3. The rate of change of the mean SMA due to thrust is given by:

$$\dot{\bar{a}}_T=\left(\frac{2\bar{a}^2v}{\mu}\right)\frac{T}{m}\underset{e\ll 1}{=}\left(\frac{2\bar{a}^{\frac{3}{2}}}{\sqrt{\mu}}\right)\frac{T}{m} \tag{42}$$

Thus,

$$\dot{V}=\Delta\bar{a}_{12}\Delta\dot{\bar{a}}_{12}=\Delta\bar{a}_{12}\left(\frac{2\bar{a}_1^{\frac{3}{2}}}{\sqrt{\mu}}\frac{T_1}{m}-\frac{2\bar{a}_2^{\frac{3}{2}}}{\sqrt{\mu}}\frac{T_2}{m}\right) \tag{43}$$

For the two controlled cases ($\Delta\bar{a}_{12}\Delta\bar{\lambda}_{12}<0$) we can replace T with the expression from Eq. (3):

$$\dot{V}=\frac{2T_{max}}{\sqrt{\mu}m}\Delta\bar{a}_{12}\left(\bar{a}_2^{\frac{3}{2}}sign\left(\Delta\bar{a}_{21}\right)-\bar{a}_1^{\frac{3}{2}}sign\left(\Delta\bar{a}_{12}\right)\right) \tag{44}$$

where $T_{max},\mu,m,\bar{a}_1,\bar{a}_2$ are all positive. To keep $\dot{V}$ continuous we approximate the $sign\left(\Delta\bar{a}\right)$ function by $\tanh\left(\frac{\Delta a}{\epsilon}\right)$ where $\epsilon\ll 1$.

$$\dot{V}=\frac{2T_{max}}{\sqrt{\mu}m}\Delta\bar{a}_{12}\left(\bar{a}_2^{\frac{3}{2}}\tanh\frac{\Delta\bar{a}_{21}}{\epsilon}-\bar{a}_1^{\frac{3}{2}}\tanh\frac{\Delta\bar{a}_{12}}{\epsilon}\right) \tag{45}$$

If $\Delta\bar{a}_{12}>0$ then $\Delta\bar{a}_{21}<0$. The first term $\frac{2T_{max}}{\sqrt{\mu}m}\Delta\bar{a}_{12}>0$ and the second term is negative so $\dot{V}<0$. If $\Delta\bar{a}_{12}<0$ then $\Delta\bar{a}_{21}>0$. The first term $\frac{2T_{max}}{\sqrt{\mu}m}\Delta\bar{a}_{12}<0$ and the second term is positive so $\dot{V}<0$.

For the two uncontrolled cases ($\Delta\bar{a}_{12}\Delta\bar{\lambda}_{12}>0$) we can replace T with zero, hance $\dot{V}=0$. This meets Eq. (41c) condition but violate Eq. (41d) condition, meaning that the controller is stable in the sense of Lyapunov but not asymptotic stable. LaSalle's invariance principle [31] shows that if we can establish that no trajectory stays identically at points where $\dot{V}\left(\Delta\bar{a}\right)=0$, except at the origin, then the origin is asymptotically stable. In modes where $\Delta\bar{a}_{12}\Delta\bar{\lambda}_{12}>0$, $\Delta\bar{\lambda}_{12}$ is always trying to change sign. When $\Delta\bar{\lambda}_{12}$ change sign the control is activated and $\dot{V}<0$. We can use LaSalle's invariance principle to show that controller Eq. (3) is in fact asymptotic stable.